International Journal of Computing and Digital Systems
ISSN (2210-142X)
Int. J. Com. Dig. Sys. 12, No.1 (Sep-2022)

https://dx.doi.org/10.12785/ijcds/120161

A Hybrid Cross Entropy Thresholding for Early Alzheimer's Disease Detection

Nancy A. Zreika[1], Ali El-Zaart[2], and Abdallah El Chakik[3]
[123]Maths. and Computer Science Department
Beirut Arab University, Beirut, Lebanon

Received 31 Mar. 2021, Revised 01 Apr. 2022, Accepted 19 Jun. 2022 Published 30 Sep. 2022

Abstract: Alzheimer's disease is an advanced form of brain disorder that touches a person' ability and disallows him to perform his daily tasks. Early diagnosis in this disease is important because it allows treatments that slow down its progression. A diagnostic indicator in patients with Alzheimer disease is the degree of generalized cerebral atrophy, revealed by MRI. The most important step in medical image diagnosis is image segmentation, which leads to precise extraction and classification. It relies on thresholding, based on the best threshold value detection that separates the background from the foreground. To estimate the best threshold value, Minimum Cross Entropy Thresholding is one of the well-known thresholding technique. To detect an optimal threshold that extracts the region reflecting the presence of the disease, we developed a novel segmentation algorithm for MRI images, using Pal method and based on a heterogeneous cross entropy thresholding technique. This technique consists of using a heterogeneous combination of 2 different statistical distributions to detect the optimal thresholding. On each image, we applied one type of distribution on the foreground and another on the background. We tried all the combinations between the statistical distributions Gaussian, Gamma, and Lognormal. Then, we confirmed validity of the proposed methodology, by using two benchmark of Alzheimer's disease images datasets, namely, OASIS-1 and OASIS-2. The hybrid combination methodology achieved more accuracy in detection, compared to other homogeneous segmentation techniques.

Keywords: Image Thresholding, Minimum Cross Entropy, PAL Method, Alzheimer MRI images, Heterogeneous Distribution.

1. Introduction

Alzheimer's disease (AD) is a brain disorder, resulting in a loss of memory and an alteration in thinking and language skills. Early treatment is essential to postpone its consequences on patients, and to maintain a certain good level of life. AD prevalence has dramatically increased worldwide, from a reported 46.8 million patients affected in 2015, to a predicted 131.5 million patients with AD in 2050 [3]. Hence, novel approaches are required to detect Alzheimer's disease at the prodromal stages. One significant issue in MRI image processing is segmentation for diagnosis of AD. Image segmentation relies on thresholding [1], which is based on the detection of the best threshold value that separates the background from the foreground. Nevertheless, difficulty remains in determining the optimal threshold value. While many segmentation models have been proposed to find an optimal threshold, they follow homogeneous distributions technique. Thus, the goal of our work is to propose a new robust and reliable methodology, heterogeneous distributions based, to obtain an optimal thresholding system, that provides consistent diagnosis, and helps physicians to detect early the disease [4]. This methodology is based on Minimum Cross Entropy Thresholding technique [1] and uses heterogeneous distributions for the detection of the disease.

The contributions in this paper are underlined as following:

- Evolving an enhanced segmentation algorithm for accurate AD detection, based on the MCET technique, and using heterogeneous distributions,
- Applying our methodology on two benchmark datasets (OASIS-1 and OASIS-2) of AD MRI images [12],
- Comparing our heterogeneous methodology with the standard homogeneous ones,
- Using the adequate performance measures to evaluate our enhanced methodology.

The paper is organized as following: Section 2, studies the related work; Section 3, describes the cross entropy thresholding technique; Section 4, introduces the statistical distributions and their properties; Section 5, describes our proposed heterogeneous model, and the proposed algorithm; Section 6, explains the performance measures used in our study; Section 7, presents the experimental results; Section 8, concludes the paper, and proposes our future work.

E-mail : [1]n.zreika@cityu.edu.lb, [2]elzaart@bau.edu.lb,[3] a.alshakik@bau.edu.lb

2. Related Work

Image segmentation is one of the most significant stages that make the computer-aided diagnosis (CAD) system reliable and effective, to be used by physicians. Several segmentation methods have been proposed to enhance AD detection, and improve diagnosis systems accuracy [5, 7, 8]. Li and Lee [1] proposed a new technique based on Minimum cross entropy thresholding technique (MCET), that optimizes the threshold value, and improves the segmentation. This technique provides better solutions for a large diversity of images that resolve NP-hard segmentation problem. Another technique, using Particle Swarm Optimization (PSO) which is based on MCET technique has been proposed by Chakraborty [5]. Using a random forests classifier, Mishra [10] proposed a new classifier model, which detects a better segmentation in skin cancer images. Al-Osaimi and El-Zaart [7], used Gamma distribution to develop a new segmentation method, to estimate an optimal thresholding system. Similarly, El-Zaart [8], used Gamma distribution to develop an improved Pal-MCET technique for bi-level and multi-level segmentation, and he applied his enhanced method on Synthetic Aperture Radar images. Also, Tan [11] proposed a new algorithm based also on PSO clustering model, to improve the performance of skin images segmentation. However, most of the aforementioned models are based on homogeneous distributions technique, while our proposed HCET (Heterogeneous Cross Entropy Thresholding) presents a novel model that combines two different statistical distributions to detect an optimum threshold value. A brain disorder such as Alzheimer's disease, requires precise segmentation. This proposed technique provides a great optimization process.

3. Image Segmentation and Thresholding Technique

Brain disorder identification is helped by image segmentation using the CAD systems, which can help physicians in patient treatment. The segmentation process guides the CAD system analysis to be accurate and reliable [11]. Some criteria are required to accomplish segmentation based on grouping image's pixels [5]. Different segmentation methods have been suggested. These follow several thresholding methods to detect the optimum segmentation. They rely on finding optimal thresholding value by separating objects from their background. Minimum Cross Entropy Gaussian distribution based, is one of the well-known thresholding technique [1]. However, when the distribution of image pixels is non-symmetric, this type of distribution is ineffective. To enhance the AD thresholding, distributions such as Gamma, Lognormal, and Beta, offer more proficiency in identifying symmetric and non-symmetric distributions.

Unlike the homogeneous distributions above, we used a hybrid model that combines between two statistical distributions, to provide a better image segmentation. The heterogeneous distributions used in our study are: Gamma/Gaussian, Gaussian/Gamma, Gamma/Lognormal, Lognormal/Gamma, Gaussian/Lognormal and Lognormal/Gaussian distributions. Note that the first distribution describes the object and the second describes the background. We applied our proposed hybrid thresholding technique on two benchmark MRI images datasets: OASIS-1 and OASIS-2 [12]. Then, we compared the results with those of the homogeneous distribution technique. Accordingly, we obtained promising experimental results.

A. Cross Entropy Thresholding

To estimate the similarity of two statistical distributions, the cross-entropy term has been proposed [8]. Thus, the cross entropy measures the theoretic distance between two distributions, and it is defined as [14]:

$$D(F, G)= \sum_{i=0}^{L-1} f_i \cdot \log\left(\frac{f_i}{g_i}\right) \quad (1)$$

where F and G refer to the sources of information, f_i and g_i are the probabilistic distributions relative to these sources while L is to the number of information values.
Mathematically, the resultant thresholded image $I_t(x, y)$ is defined as:

$$I_t(x,y)= \begin{cases} \mu_O(0,t), & I(x,y) < t \\ \mu_B(t+1, L-1), & I(x,y) \geq t \end{cases} \quad (2)$$

where I (x, y) is the original image and t is the optimum threshold.
In the thresholded image I_t, pixels are grouping into two classes: class1 = {0, 1, …, t-1} and class2 = {t, t+1, …, L-1} where class1 represents the object and class2 represents the background.

Figure 1 shows the object class and the background class of a histogram separated by a threshold line.

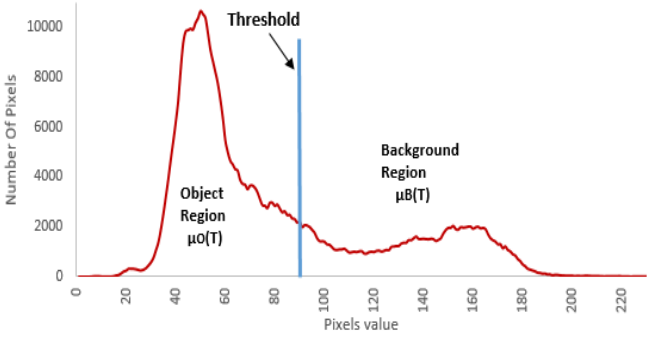

Figure 1. An example showing the object class and the background class of a histogram separated by a threshold line.

B. Minimum Cross Entropy Thresholding

To estimate the optimal threshold t^* of an image I, MCET minimizes the distance between the original image

I and the resultant segmented image I_t. Therefore, the optimal threshold t* will be as follows:

$$t^* = \arg \min_t (D(I, It)) = \arg \min_t (D(t)) \quad (3)$$

According to Li and Lee, the distance between (I) and (I_t) is defined as:

$$D(I, I_t) = \sum_{i=0}^{t} i.h(i).\log\frac{i}{\mu_O} + \sum_{i=t+1}^{L-1} i.h(i).\log\frac{i}{\mu_B} \quad (4)$$

Where i counts from 1 till 255, h(i) refers the histogram, t is the threshold value, and μ_O and μ_B are the mean values respectively of object and background regions in the original image.

Brink and Pendock assumed that the objective function of Kullback is non-symmetric and they proposed a new theoretic distance based on a true symmetric cross entropy as follows [16]:

$$D(F, G) = \sum_{i=0}^{L-1} f_i . \log\frac{f_i}{g_i} + \sum_{i=0}^{L-1} g_i . \log\frac{g_i}{f_i} \quad (5)$$

Exhaustively, the cross entropy $D_O(t)$ refers to the object region and $D_B(t)$ refers to the background region.

$$D_O(t) = D(F_O, G_O) = \sum_{i=0}^{t} f_i^o \log\left(\frac{f_i^o}{g_i^o}\right) + \sum_{i=0}^{t} g_i^o \log\left(\frac{g_i^o}{f_i^o}\right) \quad (6)$$

$$D_B(t) = D(F_B, G_B) = \sum_{i=t+1}^{L-1} f_i^B \log\left(\frac{f_i^B}{g_i^B}\right) + \sum_{i=t+1}^{L-1} g_i^B \log\left(\frac{g_i^B}{f_i^B}\right) \quad (7)$$

Thus, the total cross entropy is: $D(t) = D_O(t) + D_B(t)$ (8)

Hence, according to Brink, the total cross entropy becomes:

$$D(I, I_t) = \sum_{i=0}^{t} i.h(i).\log\frac{i}{\mu_O} + \sum_{i=t+1}^{L-1} i.h(i).\log\frac{i}{\mu_B} + \sum_{i=0}^{t} \mu_O.h(i).\log\frac{\mu_O}{i} + \sum_{i=t+1}^{L-1} \mu_B.h(i).\log\frac{\mu_B}{i} \quad (9)$$

Pal used the symmetric distance defined by Brink and Pendock in the equations (6), (7), and (8), but he assumed that each pixel in the segmented image is modeled by a statistical distribution [15], and he used Poisson distribution (respectively $g_i^O = \frac{e^{-\mu_O}}{i!}\mu_O^i$ and $g_i^B = \frac{e^{-\mu_B}}{i!}\mu_B^i$) to develop a cross entropy method that is more wide-ranging than Li and Brink.

Therefore, according to Pal, the total cross entropy is:

$$D(I, I_t) = \sum_{i=0}^{t} f_i^o \log\left(\frac{f_i^o}{g_i^o}\right) + \sum_{i=0}^{t} g_i^o \log\left(\frac{g_i^o}{f_i^o}\right) + \sum_{i=t+1}^{L-1} f_i^B \log\left(\frac{f_i^B}{g_i^B}\right) + \sum_{i=t+1}^{L-1} g_i^B \log\left(\frac{g_i^B}{f_i^B}\right) \quad (10)$$

Where, f_i^o and f_i^B are the probability distribution of pixels value in the object and background regions of the original image respectively, and calculated as follows:

$$f_i^o = \frac{h(i)}{\sum_{i=0}^{t-1} h(i)} \quad (11)$$

and

$$f_i^B = \frac{h(i)}{\sum_{i=t}^{L} h(i)} \quad (12)$$

And g_i^o and g_i^B are the probability distribution of pixels value in the object and background regions of the thresholded image respectively and estimated using Poisson distribution: $g_i^O = \frac{e^{-\mu_O}}{i!}\mu_O^i$ (13) and $g_i^B = \frac{e^{-\mu_B}}{i!}\mu_B^i$ (14)

N. Zreika & El-Zaart [17] improved the work of Pal, by assuming that the pixels in the thresholded image could be modeled by other probabilistic distributions (i.e. Gamma, Gaussian or Lognormal). They applied their enhanced methods on bi-level skin lesion images, and achieved promising results.

The previous mentioned methods are PAL Method based but they used only homogeneous distributions technique. Our goal in this paper has been to improve PAL Method more and more, by using heterogeneous distributions technique which combines two different statistical distributions.

4. Probabilistic Distributions

A histogram graphs the pixels' distribution of an image. Basically, there are two types of distribution: symmetric and non-symmetric. Gaussian distribution deals better with the symmetric shape but leads to poor segmentation results in the non-symmetric shape, whereas Gamma and Lognormal distributions represent both symmetric and non-symmetric shapes. Next, we introduced an overall description of the probabilistic distributions used in our methodology.

A. Gaussian Distribution

Gaussian distribution, represents a bell-shaped probability density curve. The following function represents Gaussian distribution [18]:

$$f(x, \mu, \sigma) = \frac{1}{\sigma\sqrt{2\pi}} e^{\frac{-1}{2}\left(\frac{x-\mu}{\sigma}\right)^2} \quad (15)$$

Where x represents the pixel's intensity level; σ is the standard deviation and μ is the mean.

Gaussian distribution can only model symmetric distributions. Therefore, μ and σ are defined as it follows [9]:

$$\mu = \frac{\sum_{i=0}^{L} i.h(i)}{\sum_{i=0}^{L} h(i)} \quad (16)$$

$$\sigma^2 = \frac{\sum_{i=0}^{L} (i-\mu)^2.h(i)}{\sum_{i=0}^{L} h(i)} \quad (17)$$

And, the distribution means of the object and the background and their standard deviations using Gaussian distribution, are respectively:

$$\mu_O = \frac{\sum_{i=0}^{t-1} i.h(i)}{\sum_{i=0}^{t-1} h(i)} \quad (18)$$

$$\mu_B = \frac{\sum_{i=t}^{L} i.h(i)}{\sum_{i=t}^{L} h(i)} \quad (19)$$

$$\sigma_O^2 = \frac{\sum_{i=0}^{t-1} (i-\mu)^2.h(i)}{\sum_{i=0}^{t-1} h(i)} \quad (20)$$

and

$$\sigma_B^2 = \frac{\sum_{i=t}^{L} (i-\mu)^2.h(i)}{\sum_{i=t}^{L} h(i)} \quad (21)$$

B. Lognormal Distribution

Lognormal distribution, whose logarithm is normally distributed, is a continuous probability distribution of a random variable. It models symmetric and moderate positively skewed distributions. The function of Lognormal distribution is defined as [19]:

$$f(x,\mu,\sigma) = \frac{1}{x\sigma\sqrt{2\pi}} e^{\frac{-1}{2}\left(\frac{\ln x-\mu}{\sigma}\right)^2} \quad (22)$$

Where x is the pixel's intensity level.
μ and σ are defined as it follows:

$$\mu = \frac{\sum_{i=0}^{L} \ln(i).h(i)}{\sum_{i=0}^{L} h(i)} \quad (23)$$

$$\sigma^2 = \frac{\sum_{i=0}^{L} (\ln(i)-\mu)^2.h(i)}{\sum_{i=0}^{L} h(i)} \quad (24)$$

Therefore, the distribution means of the object and the background and their standard deviations using Lognormal distribution, are respectively

$$\mu_O = \frac{\sum_{i=0}^{t-1} \ln(i).h(i)}{\sum_{i=0}^{t-1} h(i)} \quad (25)$$

$$\mu_B = \frac{\sum_{i=t}^{L} \ln(i).h(i)}{\sum_{i=t}^{L} h(i)} \quad (26)$$

$$\sigma_O^2 = \frac{\sum_{i=0}^{t-1} (\ln(i)-\mu)^2.h(i)}{\sum_{i=0}^{t-1} h(i)} \quad (27)$$

$$\sigma_B^2 = \frac{\sum_{i=t}^{L} (\ln(i)-\mu)^2.h(i)}{\sum_{i=t}^{L} h(i)} \quad (28)$$

C. Gamma Distribution

In statistics and probability theory, Gamma distribution stands to a continuous probability distribution of two parameters. Gamma distributions performs well in symmetric and non-symmetric histograms. The shape of Gamma distribution function can be varied from symmetric to asymmetric according to the shape parameter N. Gamma distribution function is defined by [20,21]:

$$f(x,\mu,N) = \frac{2q}{\mu}\frac{N^N}{\Gamma(N)}\left(\frac{qx}{\mu}\right)^{2N-1} e^{-N\left(\frac{qx}{\mu}\right)^2} \quad (29)$$

Where $q = \frac{\Gamma(N+0.5)}{\sqrt{N}\,\Gamma(N)}$, x is the intensity of the pixel and N is the shape parameter of the distribution. Therefore, μ is estimated as following:

$$\mu^2 = \frac{\sum_{i=0}^{L} h(i).i^2.q^2}{\sum_{i=0}^{L} h(i)} \quad (30)$$

And, object mean and background mean using Gamma distribution, are respectively

$$\mu_O^2 = \frac{\sum_{i=0}^{t-1} h(i).i^2.q^2}{\sum_{i=0}^{t-1} h(i)} \quad (31)$$

$$\mu_B^2 = \frac{\sum_{i=t}^{L} h(i).i^2.q^2}{\sum_{i=t}^{L} h(i)} \quad (32)$$

5. The proposed Hybrid Methodology

The main contribution of this study is a Heterogeneous Cross Entropy Thresholding methodology, based on PAL-MCET algorithm [15], and using heterogeneous statistical distributions. The proposed methods are described as it follows:
We considered that AD MRI image is a compound of two different distributions, one describing the object region, and another describing the background region. These distributions are varying between Gamma, Gaussian, and Lognormal. Therefore, $\mu_O(t)$ and $\mu_B(t)$ are estimated from two different distributions according to the assessed region. Hence, the histogram of the image is written as follow:

$$h(x) = P_O * dist1(x, \mu_O(t)) + P_B * dist2(x, \mu_B(t)) \quad (33)$$

such that, $dist1(x, \mu_O(t))$ is the distribution type applied on the object region and $dist2(x, \mu_B(t))$ is the distribution type applied on the background region.
Algorithm 1 presents the proposed PAL-HCET algorithm based on MCET using a heterogeneous distributions combination. The algorithm reads the original image and computes its histogram in line 1. Then, it works on each image histogram point (i.e. [0, 255]) to compute $\mu_O(t)$, $\mu_B(t)$, g_i^O, g_i^B, $D_O(t)$, $D_B(t)$ and D(t) using the different combinations of distributions. The object region average $\mu_O(t)$ and the background region average $\mu_B(t)$ are calculated using homogeneous distributions (lines 2.1-2.2-2.3) and heterogeneous distributions (lines 2.4 – 2.9). In homogeneous distributions, one type of distribution is applied on both object and background regions; while in heterogeneous distributions, one type of distribution is applied on the object region and a different type on the background region. All the possible combinations of our suggested distributions (Gaussian-Lognormal-Gamma) are used. Then, the algorithm calculates the corresponding, g_i^O, g_i^B, $D_O(t)$, $D_B(t)$ and D(t) and it searches the best threshold which minimize the distance D(t) for each of the nine combinations. Finally, the algorithm returns nine optimum thresholds relative to the nine combinations of distributions.

Proposed Algorithm: PAL-HCET Algorithm

Input: image I (x, y) //the original image

Processing:

1. Compute histogram h(i) of the input image, where pixels value counts from 0 till 255.
2. for each value of threshold t=0, ..., 255
   - 2.1. Compute $\mu_O(t)$ and $\mu_B(t)$ using Equations (18) and (19)
   - 2.2. Compute $\mu_O(t)$ and $\mu_B(t)$ using Equations (25) and (26)
   - 2.3. Compute $\mu_O(t)$ and $\mu_B(t)$ using Equations (31) and (32)
   - 2.4. Compute $\mu_O(t)$ and $\mu_B(t)$ using Equations (18) and (26)
   - 2.5. Compute $\mu_O(t)$ and $\mu_B(t)$ using Equations (18) and (32)
   - 2.6. Compute $\mu_O(t)$ and $\mu_B(t)$ using Equations (25) and (19)
   - 2.7. Compute $\mu_O(t)$ and $\mu_B(t)$ using Equations (25) and (32)
   - 2.8. Compute $\mu_O(t)$ and $\mu_B(t)$ using Equations (31) and (19)
   - 2.9. Compute $\mu_O(t)$ and $\mu_B(t)$ using Equations (31) and (26)
   - 2.10. Compute g_i^o and g_i^B based on the different combinations listed above (lines 2.1-2.9) and using respectively the heterogeneous combinations between the Equations (15-22-29).

2.11. Compute the cross entropies of the object and the background, $D_O(t)$ and $D_B(t)$, for all the combinations listed above, using equations (6) and (7).
2.12. Compute $D(t) = D_O(t) + D_B(t)$ for all the combinations using the equation (8).
2.13. Search the minimum cross entropy which minimizes the distance D(t) and its corresponding threshold.

```
If (min > D(t))
    {
  min = D(t) ;
    }
```

3. **Output**: optimal thresholds relative to nine combinations : $t_1^*, t_2^*, t_3^*, t_4^*, t_5^*, t_6^*, t_7^*, t_8^*, t_9^*$

6. Experimental Results and Discussion

In this work, we propose a hybrid segmentation technique by using heterogeneous distributions, and compare it to the benchmark techniques using homogeneous distribution. All the methods compared together are PAL Method based. We evaluate the performance of our proposed methods by testing them using two benchmark OASIS Brain datasets released by the Open Access Series of Imaging Studies (OASIS), and contains MRI data in Demented and Non Demented Older Adults. OASIS-1 is a dataset of cross-sectional MRI data, enclosing 434 scan sessions across 416 different subjects. It was made available in 2007. OASIS-2 is a dataset of longitudinal MRI data, enclosing 373 scan sessions across 150 subjects, which was made available in 2010 [12].

To evaluate the segmentation proficiency, we used 2 metrics: Image Uniformity (UN) and Region Contrast (RC) [6].

UN defines the region homogeneity in the image, and it is defined as follow:

$$UN(t) = 1 - \frac{\sigma_O^2(t) + \sigma_B^2(t)}{C} \quad (34)$$

where $\sigma_O^2(t)$ and $\sigma_B^2(t)$ are the respective variances of the object and background regions, and

$$C = \frac{(g_{max} - g_{min})^2}{2} \quad (35)$$

g_{max} and g_{min} refers to the maximum and minimum gray levels values.

UN ranges between the values 0 and 1. A value of 1 belongs to a perfect segmentation while a value of 0 belongs to a bad segmentation.

RC detects the presence of high contrast across adjacent regions in the thresholded image. The thresholded image shows a better quality when the region contrast is higher. The region contrast is defined as [6]:

$$RC(t) = \frac{|\mu_O(t) - \mu_B(t)|}{\mu_O(t) + \mu_B(t)} \quad (36)$$

Where μ_O and μ_B are respectively the mean values of the foreground and the background regions. The value of RC ranges between the values 0 and 1. A value of 1 refers to a perfect segmentation while a value of 0 refers to a bad segmentation.

The arithmetic average of UN and RC is represented by AVG, where

$$AVG = \frac{UN + RC}{2} \quad (37)$$

Tables 1, 2 and 3 show the segmentation results of 10 images selected from the two datasets after applying the proposed HCET methods. The following tables show the optimal threshold obtained and study the performance measures for each method.

Table 1 shows the results of segmentation obtained using HCET-Gamma/Gaussian, HCET-Gaussian/Gamma, MCET-Gamma and MCET-Gaussian.

Table 2 shows the results of segmentation obtained using HCET-Gamma/Lognormal and HCET-Lognormal /Gamma and then compared with MCET-Gamma and MCET- Lognormal.

Table 3 shows the performance measures and the threshold values obtained using HCET-Gaussian/Lognormal and HCET-Lognormal/Gaussian and then compared with MCET-Lognormal and MCET-Gaussian.

We notice that resulted thresholds for a particular image are distributed in a wide range, since the histogram is multimodal and the original images have low contrast.

Tables 4, 5 and 6 show a statistical study on all the images of the two datasets, the performance metrics: UN, RC and AVG, and the percentage of images ranked first for each method respectively according to UN, RC and AVG.

In table 4, for UN measure, HCET Gaussian-Gamma got first rank for 90% of all the images, MCET Gamma got first rank for only 5% of all the images, and each of MCET Gaussian and HCET Gamma-Gaussian got first rank for only 2.5% of all the images.

For RC measure, HCET Gamma-Gaussian got first rank for 55% of all the images, MCET Gaussian got first rank for only 37.5% of all the images, HCET Gaussian-Gamma got first rank for only 4% of all the images, and MCET Gamma got first rank for only 2.5% of all the images.

For AVG measure, HCET Gamma-Gaussian got first rank for 80% of all the images, HCET Gaussian-Gamma got first rank for only 15% of all the images, and each of MCET Gaussian and MCET Gamma got first rank for only 2.5% of all the images.

In table 5, for UN measure, HCET Lognormal-Gamma got first rank for 70% of all the images, MCET Gamma got first rank for 5% of the images, and each of MCET Gamma-Lognormal and MCET Lognormal got first rank for only 2.5% of all the images.

For RC measure, MCET Lognormal got first rank for 65% of all the images, HCET Gamma-Lognormal got first rank for 30% of all the images, and each of MCET Gamma and HCET Lognormal-Gamma got first rank for only 2.5% of all the images.

For AVG measure, MCET Lognormal got first rank for 65% of all the images, HCET Gamma-Lognormal got first rank for 30% of all the images, and each of MCET Gamma and HCET Lognormal-Gamma got first rank for only 2.5% of all the images.

In table 6, for UN measure, MCET Lognormal got first rank for 92.5% of all the images and each of the following methods: MCET Gaussian, HCET Gaussian-Lognormal and HCET Lognormal-Gaussian got first rank for only 2.5% of all the images.

For RC measure, HCET Gaussian-Lognormal got first rank for 90% of all the images, HCET Lognormal-Gaussian got first rank for 5% of all the images, and each of MCET Gaussian and MCET Lognormal got first rank for only 2.5% of all the images.
For AVG measure, HCET Gaussian-Lognormal got first rank for 85% of all the images, HCET Lognormal-Gaussian got first rank for 10% of all the images, and each of MCET Gaussian and MCET Lognormal got first rank for only 2.5% of all the images.
Table 7 shows a Comparison between the 9 methods MCET-Gamma, MCET-Gaussian, MCET-Lognormal, HCET-Gamma/Gaussian, HCET-Gaussian/Gamma, HCET-Gamma/Lognormal, HCET-Lognormal/Gamma, HCET-Gaussian/Lognormal, and HCET-Lognormal/Gaussian.
For UN measure, HCET Gaussian-Lognormal got first rank for 81% of all the images, HCET Gamma-Gaussian got first rank for 16% of all the images and Gamma-Lognormal got first rank for 2.5% of all the images.
For RC measure, HCET Gaussian-Lognormal got first rank for 84% of all the images, HCET Gamma-Gaussian got first rank for 6.5% of all the images and Lognormal-Gaussian got first rank for 4% of all the images.
For AVG measure, HCET Lognormal-Gamma got first rank for72% of all the images, HCET Gaussian-Gamma got first rank for 18% of all the images, and each of MCET Lognormal got first rank for 6% of all the images.

Table 1. Performance Measures: MCET-Gamma, MCET-Gaussian, HCET-Gamma/Gaussian and HCET-Gaussian/Gamma.

Image	Method	Threshold	UN	UN/Rank	RC	RC/Rank	AVG	AVG/Rank
OAS1-0002	MCET Gamma	69	0.92457	2	0.54131	3	0.73294	2
	MCET Gaussian	52	0.89112	4	0.56519	2	0.72816	3
	HCET Gamma-Gaussian	64	0.92050	3	0.56765	1	0.74407	1
	HCET Gaussian-Gamma	80	0.93160	1	0.51839	4	0.72500	4
OAS1-0010	MCET Gamma	61	0.91417	2	0.57719	3	0.74568	3
	MCET Gaussian	51	0.89354	4	0.59364	2	0.74359	4
	HCET Gamma-Gaussian	59	0.91291	3	0.59449	1	0.75370	1
	HCET Gaussian-Gamma	70	0.92045	1	0.57439	4	0.74742	2
OAS1-0020	MCET Gamma	72	0.93169	1	0.51819	3	0.72494	2
	MCET Gaussian	55	0.89660	4	0.53615	1	0.71638	4
	HCET Gamma-Gaussian	68	0.92948	3	0.52814	2	0.72881	1
	HCET Gaussian-Gamma	72	0.93169	1	0.51819	3	0.72494	2
OAS1-0050	MCET Gamma	76	0.91987	2	0.53608	2	0.72798	2
	MCET Gaussian	66	0.91112	4	0.52552	3	0.71832	4
	HCET Gamma-Gaussian	70	0.91603	3	0.55067	1	0.73335	1
	HCET Gaussian-Gamma	83	0.92284	1	0.52152	4	0.72218	3
OAS1-0100	MCET Gamma	64	0.91652	1	0.57732	4	0.74692	4
	MCET Gaussian	44	0.89634	4	0.60573	1	0.75103	2
	HCET Gamma-Gaussian	63	0.91578	2	0.57900	3	0.74739	3
	HCET Gaussian-Gamma	48	0.90126	3	0.60141	2	0.75133	1
OAS2-0009	MCET Gamma	73	0.92551	2	0.52077	3	0.72314	2
	MCET Gaussian	59	0.90390	4	0.53891	1	0.72141	3
	HCET Gamma-Gaussian	71	0.92427	3	0.52582	2	0.72504	1
	HCET Gaussian-Gamma	84	0.93077	1	0.49565	4	0.71321	4
OAS2-0014	MCET Gamma	67	0.91671	2	0.55977	3	0.73824	2
	MCET Gaussian	53	0.89060	4	0.57657	1	0.73359	3
	HCET Gamma-Gaussian	63	0.91364	3	0.57149	2	0.74256	1
	HCET Gaussian-Gamma	83	0.92586	1	0.51773	4	0.72179	4
OAS2-0021	MCET Gamma	71	0.91377	2	0.56833	3	0.74105	2
	MCET Gaussian	54	0.88326	4	0.56921	2	0.72624	4
	HCET Gamma-Gaussian	64	0.90722	3	0.58104	1	0.74413	1
	HCET Gaussian-Gamma	80	0.92030	1	0.55203	4	0.73617	3
OAS2-0098	MCET Gamma	67	0.90952	1	0.59762	3	0.75357	3
	MCET Gaussian	45	0.87762	4	0.57169	4	0.72466	4
	HCET Gamma-Gaussian	61	0.90459	2	0.60816	2	0.75638	2
	HCET Gaussian-Gamma	52	0.89519	3	0.62300	1	0.75910	1
OAS2-0102	MCET Gamma	70	0.91016	2	0.57761	2	0.74389	2

	MCET Gaussian	47	0.87079	4	0.55499	4	0.71289	4
	HCET Gamma-Gaussian	64	0.90402	3	0.58678	1	0.74540	1
	HCET Gaussian-Gamma	73	0.91244	1	0.57360	3	0.74302	3

Table 2. Performance Measures: MCET-Gamma, MCET-Lognormal, HCET-Gamma/Lognormal and HCET-Lognormal/Gamma.

Image	Method	Threshold	UN	UN/Rank	RC	RC/Rank	AVG	AVG/Rank
OAS1-0002	MCET Gamma	69	0.92457	3	0.54131	2	0.73294	2
	MCET Lognormal	97	0.93754	1	0.48559	4	0.71156	4
	HCET Gamma-Lognormal	66	0.92215	4	0.54816	1	0.73515	1
	HCET Lognormal-Gamma	80	0.93160	2	0.51839	3	0.72500	3
OAS1-0010	MCET Gamma	61	0.91417	1	0.57719	2	0.74568	2
	MCET Lognormal	51	0.90645	4	0.60439	1	0.75542	1
	HCET Gamma-Lognormal	61	0.91417	1	0.57719	2	0.74568	2
	HCET Lognormal-Gamma	61	0.91417	1	0.57719	2	0.74568	2
OAS1-0020	MCET Gamma	72	0.93169	3	0.51819	1	0.72494	1
	MCET Lognormal	77	0.93387	1	0.50650	3	0.72018	3
	HCET Gamma-Lognormal	72	0.93169	3	0.51819	1	0.72494	1
	HCET Lognormal-Gamma	77	0.93387	1	0.50650	3	0.72018	3
OAS1-0050	MCET Gamma	76	0.91987	2	0.53608	1	0.72798	1
	MCET Lognormal	85	0.92343	1	0.51762	3	0.72052	3
	HCET Gamma-Lognormal	76	0.91987	2	0.53608	1	0.72798	1
	HCET Lognormal-Gamma	85	0.91310	4	0.51762	3	0.71536	4
OAS1-0100	MCET Gamma	64	0.91652	1	0.57732	4	0.74692	4
	MCET Lognormal	48	0.90126	4	0.60141	1	0.75133	1
	HCET Gamma-Lognormal	63	0.91578	2	0.57900	3	0.74739	3
	HCET Lognormal-Gamma	58	0.91154	3	0.58724	2	0.74939	2
OAS2-0009	MCET Gamma	73	0.92551	4	0.52077	1	0.72314	1
	MCET Lognormal	90	0.93235	1	0.48307	4	0.70771	4
	HCET Gamma-Lognormal	78	0.92838	3	0.50837	2	0.71837	2
	HCET Lognormal-Gamma	84	0.93077	2	0.49565	3	0.71321	3
OAS2-0014	MCET Gamma	67	0.91671	2	0.55977	3	0.73824	3
	MCET Lognormal	58	0.90966	4	0.58554	1	0.74760	1
	HCET Gamma-Lognormal	63	0.91364	3	0.57149	2	0.74256	2
	HCET Lognormal-Gamma	81	0.92500	1	0.52261	4	0.72381	4
OAS2-0021	MCET Gamma	71	0.91377	3	0.56833	2	0.74105	2
	MCET Lognormal	80	0.92030	2	0.55203	3	0.73617	3
	HCET Gamma-Lognormal	67	0.91032	4	0.57528	1	0.74280	1
	HCET Lognormal-Gamma	81	0.92092	1	0.55014	4	0.73553	4
OAS2-0098	MCET Gamma	67	0.90952	1	0.59762	4	0.75357	4
	MCET Lognormal	52	0.89519	4	0.62308	1	0.75914	1
	HCET Gamma-Lognormal	62	0.90545	2	0.60649	2	0.75597	2
	HCET Lognormal-Gamma	62	0.90545	2	0.60649	2	0.75597	2
OAS2-0102	MCET Gamma	70	0.91016	2	0.57761	3	0.74389	3
	MCET Lognormal	55	0.89300	4	0.60024	1	0.74662	1
	HCET Gamma-Lognormal	64	0.90402	3	0.58678	2	0.74540	2

	HCET Lognormal-Gamma	82	0.91902	1	0.55954	4	0.73928	4

Table 3. Performance Measures: MCET-Gaussian, MCET-Lognormal, HCET-Gaussian/Lognormal and HCET-Lognormal/Gaussian.

Image	Method	Threshold	UN	UN/Rank	RC	RC/Rank	AVG	AVG/Rank
OAS1-0002	MCET Gaussian	52	0.89112	4	0.56519	3	0.72816	3
	MCET Lognormal	97	0.93754	1	0.48559	4	0.71156	4
	HCET Gaussian-Lognormal	45	0.90063	3	0.59650	1	0.74857	1
	HCET Lognormal-Gaussian	52	0.90896	2	0.58028	2	0.74462	2
OAS1-0010	MCET Gaussian	51	0.89354	4	0.59364	4	0.74359	4
	MCET Lognormal	51	0.90645	1	0.60439	2	0.75542	2
	HCET Gaussian-Lognormal	43	0.89823	3	0.62602	1	0.76212	1
	HCET Lognormal-Gaussian	51	0.90645	1	0.60439	2	0.75542	2
OAS1-0020	MCET Gaussian	55	0.89660	4	0.55615	2	0.72638	3
	MCET Lognormal	77	0.93387	1	0.50650	4	0.72018	4
	HCET Gaussian-Lognormal	49	0.91391	3	0.58059	1	0.74725	1
	HCET Lognormal-Gaussian	68	0.92948	2	0.52814	3	0.72881	2
OAS1-0050	MCET Gaussian	66	0.91112	3	0.52552	3	0.71832	4
	MCET Lognormal	85	0.92343	1	0.51762	4	0.72052	3
	HCET Gaussian-Lognormal	55	0.90295	4	0.58845	1	0.74570	1
	HCET Lognormal-Gaussian	66	0.91310	2	0.56060	2	0.73685	2
OAS1-0100	MCET Gaussian	44	0.89634	3	0.60573	1	0.75103	3
	MCET Lognormal	48	0.90126	2	0.60141	2	0.75133	2
	HCET Gaussian-Lognormal	46	0.88722	4	0.56956	4	0.72839	4
	HCET Lognormal-Gaussian	51	0.90844	1	0.59985	3	0.75414	1
OAS2-0009	MCET Gaussian	59	0.90390	4	0.53891	3	0.72141	3
	MCET Lognormal	90	0.93235	1	0.48307	4	0.70771	4
	HCET Gaussian-Lognormal	59	0.91498	2	0.55854	1	0.73676	1
	HCET Lognormal-Gaussian	59	0.91498	2	0.55854	1	0.73676	1
OAS2-0014	MCET Gaussian	53	0.89060	4	0.57657	4	0.73359	4
	MCET Lognormal	58	0.90966	1	0.58554	3	0.74760	3
	HCET Gaussian-Lognormal	47	0.89926	3	0.61658	1	0.75792	1
	HCET Lognormal-Gaussian	53	0.90521	2	0.59995	2	0.75258	2
OAS2-0021	MCET Gaussian	54	0.88326	4	0.56921	2	0.72624	4
	MCET Lognormal	80	0.92030	1	0.55203	4	0.73617	3
	HCET Gaussian-Lognormal	50	0.88911	3	0.60979	1	0.74945	1
	HCET Lognormal-Gaussian	71	0.91377	2	0.56833	3	0.74105	2
OAS2-0098	MCET Gaussian	45	0.87762	4	0.57169	4	0.72466	4
	MCET Lognormal	52	0.89519	1	0.62308	3	0.75914	3
	HCET Gaussian-Lognormal	44	0.88338	3	0.63561	1	0.75949	1
	HCET Lognormal-Gaussian	51	0.89395	2	0.62468	2	0.75931	2
OAS2-0102	MCET Gaussian	47	0.87079	4	0.55499	4	0.71289	4
	MCET Lognormal	55	0.89300	1	0.60024	3	0.74662	2
	HCET Gaussian-Lognormal	45	0.87768	3	0.61349	1	0.74559	3
	HCET Lognormal-Gaussian	52	0.88894	2	0.60434	2	0.74664	1

Table 4. Performance Measures Evaluation for the 4 Methods: MCET-Gamma, MCET-Gaussian, HCET-Gamma/Gaussian and HCET-Gaussian/Gamma.

Method	%UN	%RC	%AVG
MCET Gamma	5%	2.5%	2.5%
MCET Gaussian	2.5%	37.5%	2.5%
HCET Gamma-Gaussian	2.5%	55%	80%
HCET Gaussian-Gamma	90%	4%	15%

Table 5. Performance Measures Evaluation for the 4 Methods: MCET-Gamma, MCET-Lognormal, HCET-Gamma/Lognormal and HCET-Lognormal/Gamma.

Method	%UN	%RC	%AVG
MCET Gamma	5.0%	2.5%	2.5%
MCET Lognormal	2.5%	65.0%	65.0%
HCET Gamma-Lognormal	2.5%	30.0%	30.0%
HCET Lognormal-Gamma	70.0%	2.5%	2.5%

Table 6. Performance Measures Evaluation for the 4 Methods: MCET-Gaussian, MCET-Lognormal, HCET-Gaussian/Lognormal and HCET-Lognormal/Gaussian.

Method	%UN	%RC	%AVG
MCET Gaussian	2.5%	2.5%	2.5%
MCET Lognormal	92.5%	2.5%	2.5%
HCET Gaussian-Lognormal	2.5%	90.0%	85.0%
HCET Lognormal-Gaussian	2.5%	5.0%	10.0%

Table 7. Comparison between the 9 methods (Homogeneous and Heterogeneous Distributions based): MCET-Gamma, MCET-Gaussian, MCET-Lognormal, HCET-Gamma/Gaussian, HCET-Gaussian/Gamma, HCET-Gamma/Lognormal, HCET-Lognormal/Gamma, HCET-Gaussian/Lognormal, and HCET-Lognormal/Gaussian.

Method	%UN	UN/Rank	%RC	RC/Rank	%AVG	AVG/Rank
MCET Gamma	0.30%	7	0.00%	7	0.10%	6
MCET Gaussian	0.10%	8	0.00%	7	0.00%	9
MCET Lognormal	6.00%	3	3.50%	4	1.00%	4
HCET Gamma-Gaussian	1.00%	5	6.50%	2	16.00%	2
HCET Gaussian-Gamma	18.00%	2	0.00%	7	0.10%	6
HCET Gamma-Lognormal	1.50%	4	1.00%	5	1.50%	3
HCET Lognormal-Gamma	72.00%	1	1.00%	5	0.10%	6
HCET Gaussian-Lognormal	1.00%	5	84.00%	1	81.00%	1
HCET Lognormal-Gaussian	0.10%	8	4.00%	3	0.20%	5

Figure 2, Figure 3, Figure 4 and *Figure* 5 show a sample of tested images and their resulting segmentation using our enhanced methodology. Each figure contains the original image (a), the thresholded images respectively resulting from MCET-Gamma (b), MCET-Gaussian (c), MCET- Lognormal (d), HCET- Gamma/Gaussian (e), HCET-Gaussian/Gamma(f), HCET- Gamma/Lognormal (g), HCET-Lognormal/Gamma (h), HCET- Gaussian/Lognormal (i), HCET-Lognormal/Gaussian (j). The graph (k) shows the histogram of the image, and the value of thresholds found in each method (l).

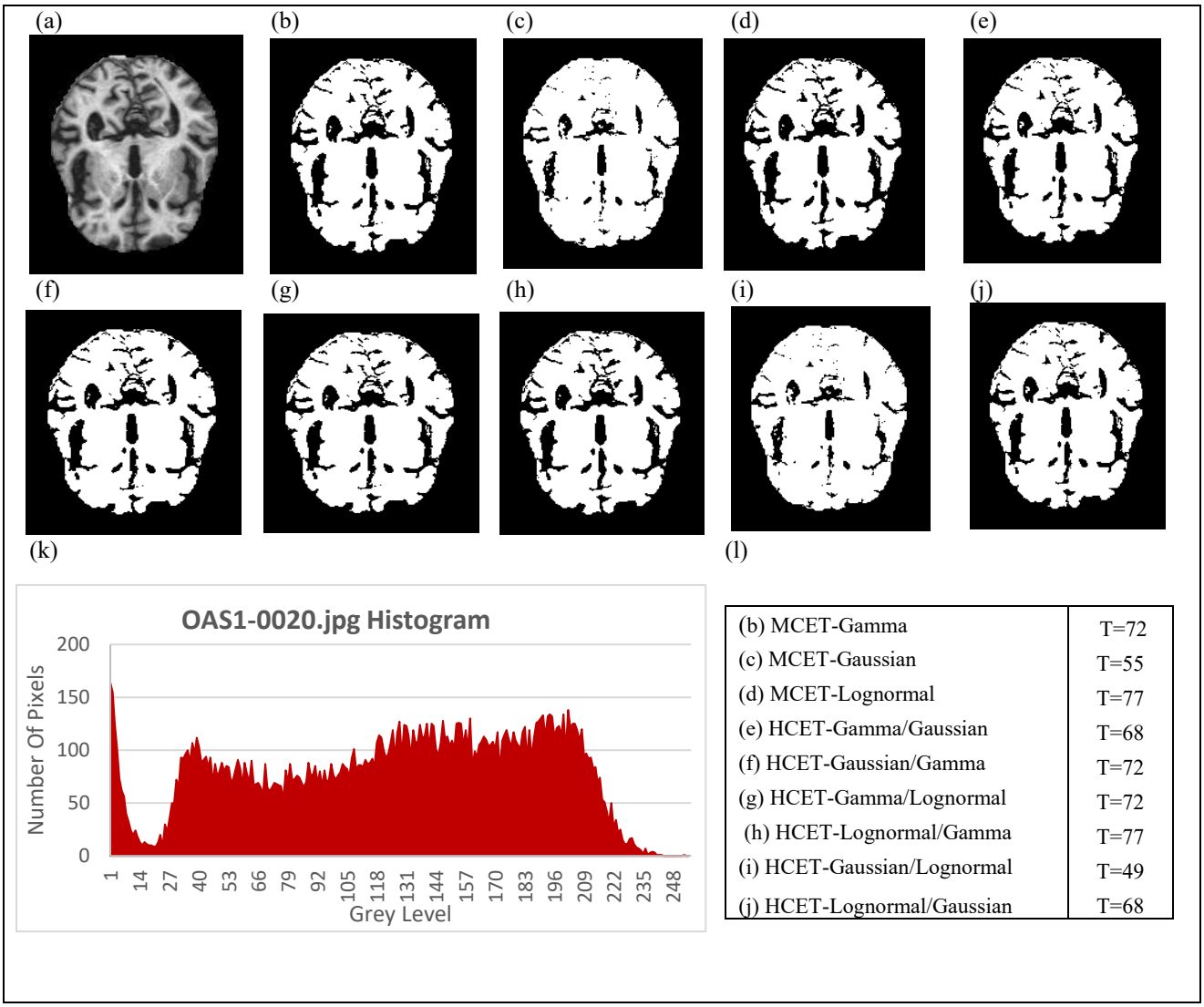

(b) MCET-Gamma	T=72
(c) MCET-Gaussian	T=55
(d) MCET-Lognormal	T=77
(e) HCET-Gamma/Gaussian	T=68
(f) HCET-Gaussian/Gamma	T=72
(g) HCET-Gamma/Lognormal	T=72
(h) HCET-Lognormal/Gamma	T=77
(i) HCET-Gaussian/Lognormal	T=49
(j) HCET-Lognormal/Gaussian	T=68

Figure 1. (a)Original Image OAS1-0020. (b) Segmented Image using MCET-Gamma. (c) Segmented Image using MCET-Gaussian. (d) Segmented Image using MCET-Lognormal**.** (e) Segmented Image using HCET- Gamma/Gaussian**.** (f) Segmented Image using HCET- Gaussian/Gamma. (g) Segmented Image using HCET- Gamma/Lognormal. (h) Segmented Image using HCET-Lognormal/Gamma. (i) Segmented Image using HCET- Gaussian/Lognormal. (j) Segmented Image using HCET-Lognormal/Gaussian. (k) Histogram of OAS1-0020 image. (l) The threshold value found in each method.

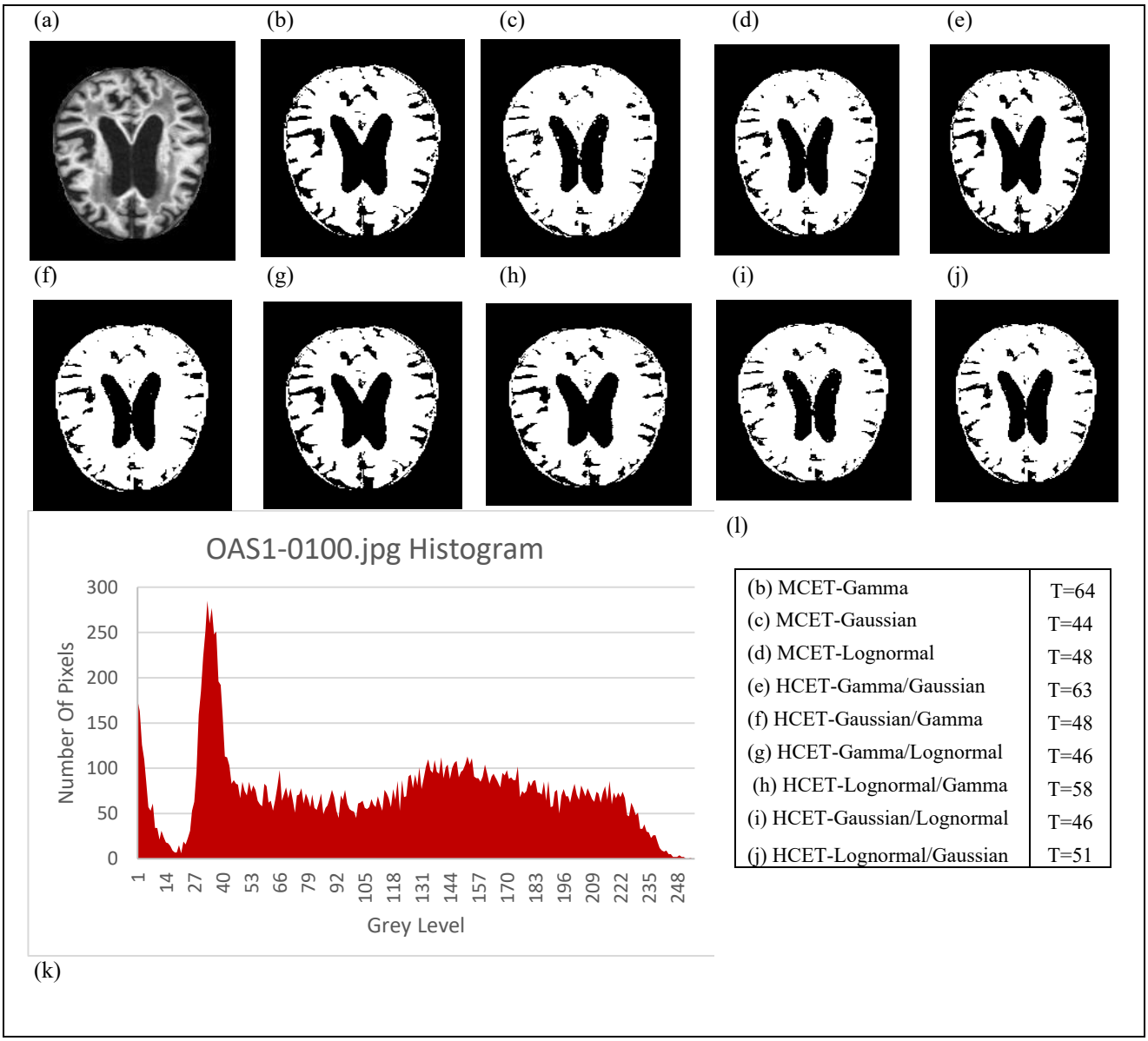

Figure 2. (a)Original Image OAS1-0100. (b) Segmented Image using MCET-Gamma. (c) Segmented Image using MCET-Gaussian. (d) Segmented Image using MCET-Lognormal. (e) Segmented Image using HCET- Gamma/Gaussian. (f) Segmented Image using HCET- Gaussian/Gamma. (g) Segmented Image using HCET- Gamma/Lognormal. (h) Segmented Image using HCET-Lognormal/Gamma. (i) Segmented Image using HCET- Gaussian/Lognormal. (j) Segmented Image using HCET-Lognormal/Gaussian. (k) Histogram of OAS1-0100 image. (l) The threshold value found in each method.

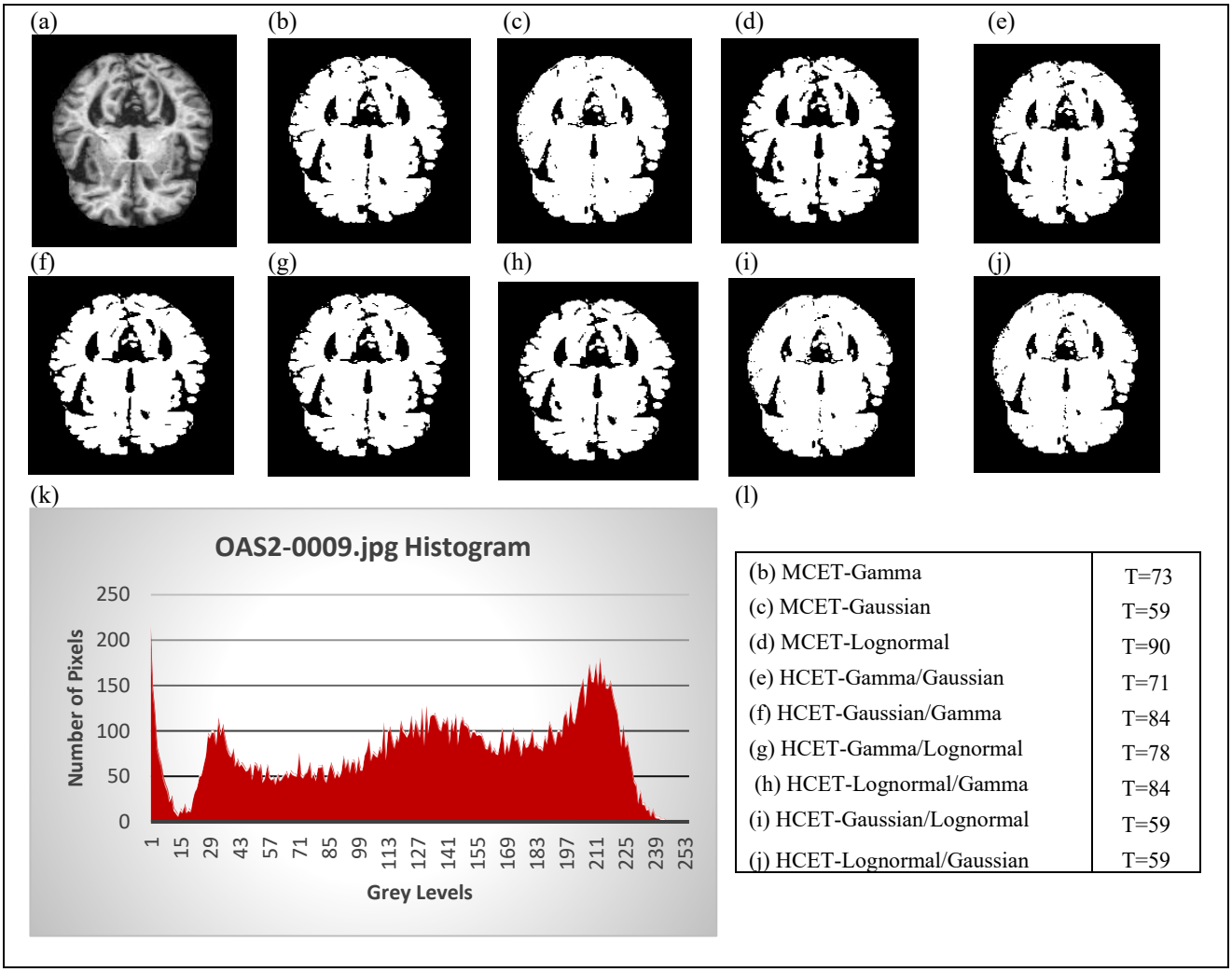

Figure 3. (a)Original Image OAS2-0009. (b) Segmented Image using MCET-Gamma. (c) Segmented Image using MCET-Gaussian. (d) Segmented Image using MCET-Lognormal**.** (e) Segmented Image using HCET- Gamma/Gaussian**.** (f) Segmented Image using HCET- Gaussian/Gamma. (g) Segmented Image using HCET- Gamma/Lognormal. (h) Segmented Image using HCET-Lognormal/Gamma. (i) Segmented Image using HCET- Gaussian/Lognormal. (j) Segmented Image using HCET-Lognormal/Gaussian. (k) Histogram of OAS2-0009 image. (l) The threshold value found in each method.

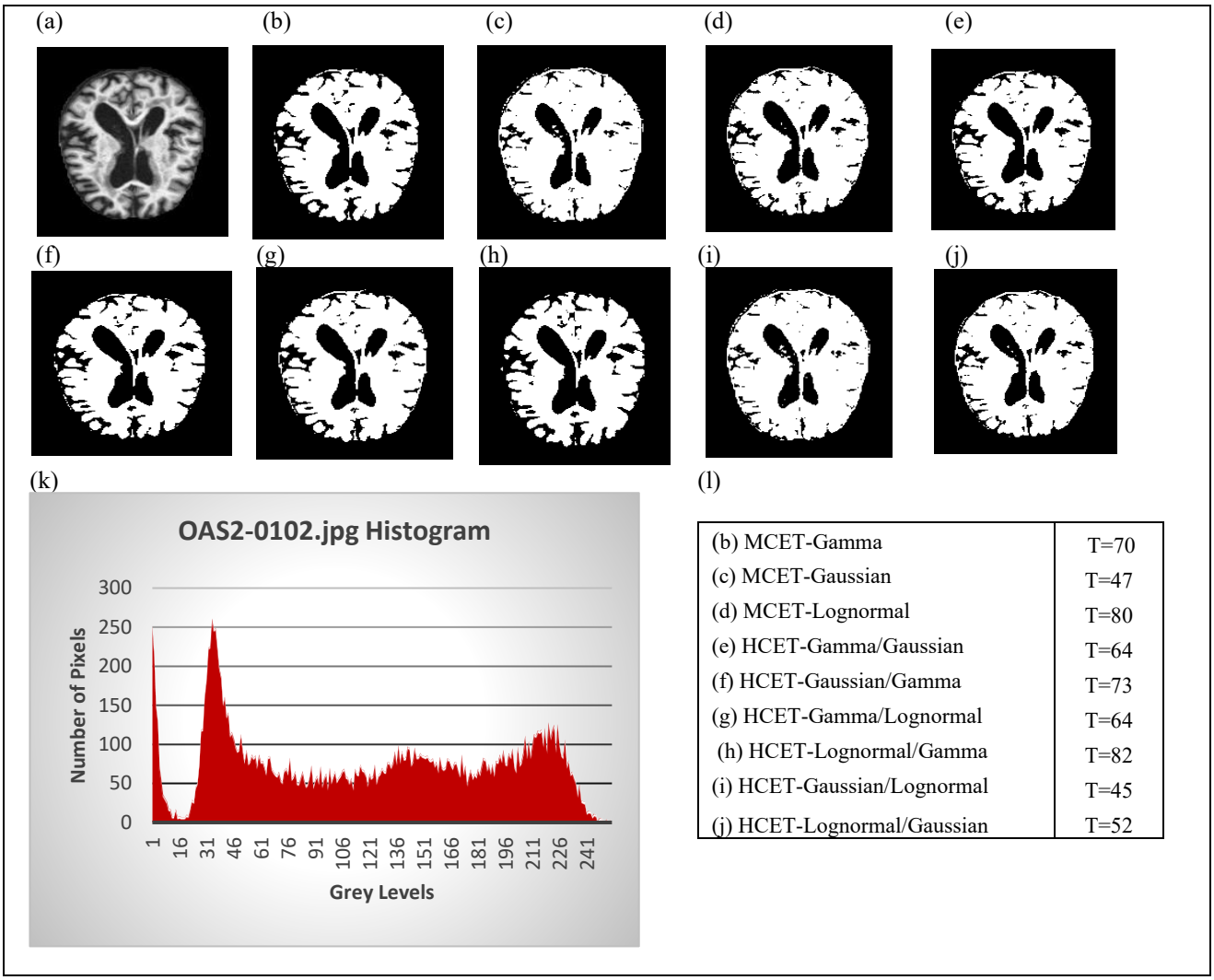

Figure 4. (a)Original Image OAS2-0102. (b) Segmented Image using MCET-Gamma. (c) Segmented Image using MCET-Gaussian. (d) Segmented Image using MCET-Lognormal. (e) Segmented Image using HCET- Gamma/Gaussian. (f) Segmented Image using HCET- Gaussian/Gamma. (g) Segmented Image using HCET- Gamma/Lognormal. (h) Segmented Image using HCET-Lognormal/Gamma. (i) Segmented Image using HCET- Gaussian/Lognormal. (j) Segmented Image using HCET-Lognormal/Gaussian. (k) Histogram of OAS2-0102 image. (l) Threshold value found in each method.

7. Conclusion and Future Work:

This work proposed a new performed segmentation method based on MCET technique, defined by PAL and using heterogeneous statistical distributions to find best segmentation for MRI AD images. The efficiency of the proposed methodology is tested using two Oasis Brain datasets [12]. As shown, the suggested Heterogeneous Cross Entropy Thresholding methods (PAL-HCET) using the combination Gaussian/Lognormal empirically outperformed other homogeneous segmentation methods.

The result of the experiment, in Table 7, shows that 81% of the tested images are better segmented using the heterogeneous combination of statistical distributions Gaussian-Lognormal, also around 99% of the tested images confirmed that AD images histogram is a combination of heterogeneous distributions.

Therefore, the proposed Heterogeneous Cross Entropy Thresholding model is a robust model and surpasses the other classical segmentation methods.

Future work will aim to cover other domains such as, skin cancer images, radar images, industrial images, and satellite images. Moreover, we will extend PAL-HCET contribution to include multi-level images.

Acknowledgment:

I would like to express my gratitude to Dr. Ali El-Zaart for his valuable and productive suggestion during the planning and development of this research work.

I would also like to acknowledge Dr. Abdallah El Shakik for his appreciated technical support.

References:

[1] C. Li and C. Lee (1993), "Minimum cross entropy thresholding," Pattern Recognition, vol. 26, no. 4, pp. 617–625.

[2] J.C. Russ, "The image processing handbook," CRC Press, Boca Raton, NW, USA, 5th edition, 2007.

[3] Dementia statistics, Alzheimer's Disease International, https://www.alz.co.uk/research/statistics.

[4] Hala Al-Shamlan, Ali El-Zaart, Breast Cancer Computer aided Detection (CAD) System, Proceedings of the International Conference on Image Processing, Computer Vision, and Pattern Recognition (IPCV), 2011.

[5] Chakraborty, Rupak, Rama Sushil, and M. L. Garg. "An improved PSO-based multilevel image segmentation technique using minimum cross-entropy thresholding." Arabian Journal for Science and Engineering 44.4 (2019): 3005-3020.

[6] Mehmet Sezgin and Bulent Sankur (2004), "Survey over image thresholding techniques and quantitative performance evaluation," Journal of Electronic Imaging., pp. 146–168.

[7] Ghada Al-Osaimi, Ali El-Zaart, 2008 3rd International Conference on Information and Communication Technologies: From Theory to Applications.: April 2008pages:1-6

[8] Amani Al-Ajlan, Ali El-Zaart, Image segmentation using minimum cross-entropy thresholding, 2009 IEEE International Conference on Systems, Man and Cybernetics, 1776-178, 2009.

[9] Li, Jiafu, et al. "A multilevel color image thresholding scheme based on minimum cross entropy and alternating direction method of multipliers." Optik 183 (2019): 30-37.

[10] Mishra, Nabin K., et al. "Automatic lesion border selection in dermoscopy images using morphology and color features." Skin Research and Technology (2019).

[11] Tan, Teck Yan, et al. "Evolving Ensemble Models for Image Segmentation Using Enhanced Particle Swarm Optimization." IEEE Access (2019).

[12] OASIS BRAINS – Open Access Series of Imaging Studies, Datasets of Alzheimer's disease MRI Images, http://www.oasis-brains.org

[13] C.H.Li and P K S Tam (1998), "An iterative algorithm for minimum cross entropy thresholding", Pattern Recognition Vol 19, pp 771-776

[14] S. Kullback (1959), Information Theory and Statistics. Wiley, New York.

[15] Pal, N. (1996), "On Minimum cross entropy thresholding," Pattern Recognition Letter, vol. 29 no. 4, pp. 575–580.

[16] A. Brink, and N. Pendock, "Minimum Cross-entropy Threshold Selection," Pattern Recognition Letter - Elsevier, vol. 29, no. 1, 1996, pp. 179-188.

[17] An improvement of Cross Entropy Thresholding for Skin Cancer Detection, Nancy A. Zreika, Ali El-Zaart, Abdallah Al Shakik, © BAU Journal – Beirut Arab University, Lebanon, 2020. (Accepted)

[18] G.McPherson,"Statistics in scientific investigation: its basis, application and interpretation", Springer-Verlag,1990.

[19] C. Forbes, et al., "Statsitical Distributions" 4th edition, John wiley & Sons, 2011.

[20] C.H.Li and P K S Tam (1998) "An iterative algorithm for minimum cross entropy thresholding", Pattern Recognition Vol 19, pp 771-776.

[21] ŞENGÜR, I. TÜRKOĞLU and M. İNCE (2006), "A Comparative Study On Entropic Thresholding Methods" Journal of Electrical & Electronics Engineering, vol.6, no. 2, pp. 183-188.

[22] Sun, Hao, Xianqiang Yang, and Huijun Gao. "A spatially constrained shifted asymmetric Laplace mixture model for the grayscale image segmentation." Neuro computing 331 (2019): 50-57.

[23] Rezaee, Mohammad, and Daniel Letourneau. "Assessment of Image Quality and Dosimetric Performance of CT Simulators." Journal of Medical Imaging and Radiation Sciences (2019).

[24] M.D. Levine and A.M. Nazif. Dynamic measurement of computer generated image segmentations. Pattern Analysis and Machine Intelligence, IEEE Transactions on, (2): 155–164, 1985.

[25] Zhang, Jie, Bowen Zheng, Ang Gao, Xin Feng, Dong Liang, and Xiaojing Long. "A 3D densely connected convolution neural network with connection-wise attention mechanism for Alzheimer's disease classification." Magnetic Resonance Imaging 78 (2021): 119-126.

[26] Liu, M., Li, F., Yan, H., Wang, K., Ma, Y., Shen, L., ... & Alzheimer's Disease Neuroimaging Initiative. (2020). A multi-model deep convolutional neural network for automatic hippocampus segmentation and classification in Alzheimer's disease. Neuroimage, 208, 116459.

[27] Yew, A. Y. L., & Rahim, M. S. M. (2021). Dimensionality Reduction Methods for Alzheimer's Disease Classification. International Journal of Computing and Digital Systems, 10.

Author Biographies

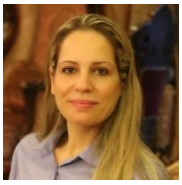

Nancy A. Zreika received a BSc in Information Technology from Lebanese University, Tripoli, Lebanon in 2001, and M.Sc. degree in Information Technology, Computer Science Department from the University of Balamand, Lebanon in 2007. Her master thesis includes a Speaker Verification System for voice recognition. She is pursuing actually a PHD at Beirut Arab University, Beirut, Lebanon. She is a lecturer at City University- Tripoli, Lebanon, and at High Official Technical School of Tripoli. Her research interests include image processing, machine learning and computer vision.

Ali El-Zaart is an associate professor at the Beirut Arab University. He received a BSc in computer science from Lebanese University - Beirut, Lebanon in 1990, M.Sc. degree in computer science from the University of Sherbrooke, Sherbrooke, Canada in 1996, and Ph.D. degree in computer science from the University of Sherbrooke, Sherbrooke, Canada in 2001. His research interests include image processing, pattern recognition, remote sensing, and computer vision.

Abdallah El Chakik received a Ph.D. in 2014 and a M.S. degree in computer science in 2010, from the University of Caen, France. He obtained his B.S. in computer science from Saint Etienne University-France in 2006. He is an Associate Professor in CS Department at Beirut Arab University. His research interests include image and signal processing applications and computer vision.